HiSST: 2nd International Conference on High-Speed Vehicle Science & Technology
11–15 September 2022, Bruges, Belgium

Liquid Ablation Measurement in the ISL's Hypersonic Shock Tunnels

Flavien DENIS[1], *Robert HRUSCHKA*[2]

Abstract

At hypersonic speed, the metallic parts of flight vehicles are ablated by melting and by oxidation. A novel experimental method is presented, which aims to investigate the ablation by melting in hypersonic impulse facilities. The combination of a low melting point metal with a direct visualization method allows the measurement of ablation profiles in steady hypersonic flows of only two milliseconds. The ablation profiles obtained for a hypersonic flow of nitrogen at Mach 4.5 are presented and discussed. For the tested conditions, the location of the ablation maximum is never located at the stagnation point but rather at 30° from the symmetry axis. Comparisons with CFD simulations demonstrate that the contribution of the ablation by erosion is a secondary phenomenon compared to that of the ablation by melting. Moreover the shape of the ablation profiles can be explained by the laminar-turbulent transition in the boundary layer between the locations of $10°$ and $20°$ from the stagnation point.

Keywords: *liquid ablation, hypersonic flow, shock tunnel, CFD*

Nomenclature

Latin

Cp – Heat capacity $[J \cdot kg^{-1} \cdot K^{-1}]$
D – Hemisphere diameter $[m]$
d – Surface displacement $[m]$
h – Equivalent altitude $[km]$ or enthalpy $[J \cdot kg^{-1}]$
k – Turbulence kinetic energy $[m^2 \cdot s^{-2}]$
M – Mach number $[-]$
P – Pressure $[Pa]$
q_w – Wall heat flux $[W \cdot m^{-2}]$
Re/x – Reynolds number per unit length $[m^{-1}]$
Re_θ – Transition momentum thickness Reynolds number $[-]$
T – Temperature $[K]$
Tu – Turbulence intensity $[-]$
u – Freestream velocity $[m \cdot s^{-1}]$
x – Horizontal position $[m]$
y – Vertical position $[m]$

Greek

α_t – Turbulence thermal diffusivity $[kg \cdot m^{-1} \cdot s^{-1}]$
θ – Position angle on the model $[°]$
ΔH – Latent heat $[J \cdot kg^{-1}]$
γ – Intermittency $[-]$
λ – Thermal heat conductivity $[W \cdot m^{-1} \cdot K^{-1}]$
ω – Turbulence dissipation $[s^{-1}]$
ν_t – Turbulence viscosity $[m^2 \cdot s^{-1}]$
τ – Wall shear stress $[Pa]$
ρ – Density $[kg \cdot m^{-3}]$
σ_{el} – Yield strength $[Pa]$
σ_{ts} – Tensile strength $[Pa]$

Subscripts

∞ – Freestream value
0 – Stagnation value
f – Fusion
Ga – Gallium
max – Maximum value
S – Sublimation

Acronyms

CFD – Computational Fluid Dynamics
ISL – French-German Research Institute of Saint-Louis
SST – Shear Stress Transport
STB – ISL shock tunnel B

[1]*Aerodynamics, Measurements & Simulations, French-German Research Institute of Saint-Louis, 5 rue du Général Cassagnou - BP 70034, 68301 Saint-Louis Cedex - France, flavien.denis@isl.eu*
[2]*Aerodynamics, Measurements & Simulations, French-German Research Institute of Saint-Louis, 5 rue du Général Cassagnou - BP 70034, 68301 Saint-Louis Cedex - France, robert.hruschka@isl.eu*

1. Introduction

The liquid ablation, also called ablation by melting, refers to the degradation phenomenon, which leads to the degradation of the hypersonic vehicle surfaces by melting and oxidation due to the high temperature and the high thermal load on the vehicle surfaces. It particularity affects all surfaces made of metallic materials, which are not protected from the heat by a thermal protection system. Most of the experimental studies regarding this phenomenon were performed in the 60s by using experimental facilities such as ballistic ranges [1] and plasma torches [2]. Even if most studies involving the liquid ablation are today numerical studies, experimental data are still needed for the calibration and the validation of these numerical tools. Moreover, new hypersonic vehicles such as future hypersonic cruise missiles and hypersonic projectiles will fly at low altitude and therefore require experimental data for the ablation phenomenon in dense flows.

In the present paper, a novel approach for the investigation of the liquid ablation in such flows within a hypersonic impulse facility is presented. The measured ablation profiles are compared with numerical results obtained with an OpenFOAM based CFD solver.

2. Experimental setup

2.1. High enthalpy shock tunnel

The ablation experiments are carried out within the ISL high enthalpy shock tunnel STB. This is a hypersonic impulse facility able to generate hypersonic flows up to Mach 14 and up to a total enthalpy of $8MJ \cdot kg^{-1}$. For the present study, four flow conditions are selected with a Mach number of 4.5 and total enthalpies ranging from 1.3 to $1.8MJ \cdot kg^{-1}$. Nitrogen is used as test gas in order to avoid any oxidation on the model surface and hence to study the ablation by melting only. Table 1 summarizes the flow conditions. The Mach number 4.5 is used in order to maximize the wall heat flux on the model surface for flow conditions with the highest flow density corresponding to the equivalent altitudes of $h = 1km$ and $h = 3km$. For these flow conditions, the measured steady flow durations are about two milliseconds.

Table 1. Flow conditions for the ablation experiments

Condition n°	M_∞ (-)	h (km)	Re/x (m^{-1})	u_∞ $(m \cdot s^{-1})$	T_∞ (K)	P_∞ (Pa)	T_0 (K)	h_0 $(J \cdot kg^{-1})$
1	4.43	3	4.95 E+7	1670	343	6.94 E+4	1450	1.76 E+6
2	4.51	1	9.06 E+7	1500	265	9.00 E+4	1160	1.40 E+6
3	4.53	6	5.86 E+7	1440	244	5.20 E+4	1070	1.29 E+6
4	4.51	13	1.73 E+7	1460	252	1.61 E+4	1090	1.32 E+6

2.2. Gallium model

In the ISL shock tunnel, the metals classically used for aerospace applications, such as aluminium alloys, titanium alloys or Inconel cannot be ablated within the steady flow duration. Therefore, a suitable substitute ablative material has to be found. Some of these were already used in previous studies such as water ice [3], dry ice [4] or naphthalene [5], but are not well suited for use in the shock tunnel, as they partially melt or evaporate during the test preparation. Finally, the gallium, a non-toxic low melting point metal is chosen as ablative material, because of its low melting point of only $302K$. In the shock tunnel, it melts quickly after the steady flow start and the use of nitrogen as test gas allows the measurement of pure ablation by melting, i.e. without oxidation and without evaporation phenomena. The main properties of gallium are summarized in Table 2.

Table 2. Gallium properties for the solid phase (from [6] and [7])

ρ_{Ga} $(kg \cdot m^{-3})$	Cp_{Ga} $(J \cdot kg^{-1} \cdot K^{-1})$	λ_{Ga} $(W \cdot m^{-1} \cdot K^{-1})$	$\Delta H_{f,Ga}$ $(J \cdot kg^{-1})$	$T_{f,Ga}$ (K)	$T_{s,Ga}$ (K)	σ_{el} (MPa)	σ_{ts} (MPa)
5904	370	41	80200	302.9	2477	8-25	15-40

The three geometries studied are shown in Figure 1: a 8mm-hemisphere-cone model, a 10mm-hemisphere cone model and a 14mm-hemisphere model. Due to the low melting point of gallium, the models are generated by casting. The liquid gallium is directly cast on the sting by the use of 3D-printed molds. The model is then polished in order to obtain a smooth surface.

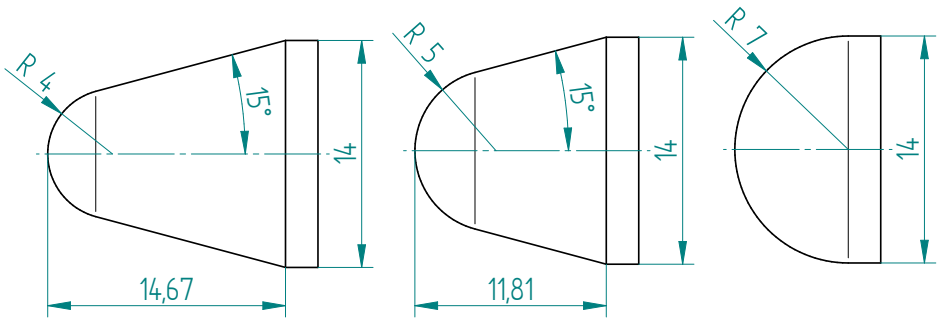

Fig 1. 8mm-, 10mm- and 14mm-hemisphere model geometries

2.3. Direct visualization and post-treatment

The ablation profiles are measured optically through a direct visualization method as shown in Figure 2. On one side of the test section, a flash lamp with a light diffuser illuminates the model. On the other side of the test section, the combination of two camera lenses and a beam splitter allows two visualizations of the model surface with two high speed cameras Photron SAZ at $12500 frames \cdot s^{-1}$ with the same line of sight but with two magnification levels. The entire gallium model and part of the sting are visible on the low magnified video with a resolution of $0.02mm \cdot px^{-1}$. The highly magnified video reaches a resolution of $0.005mm \cdot px^{-1}$ and visualizes the stagnation point in order to precisely measure the surface recession caused by the ablation in this region.

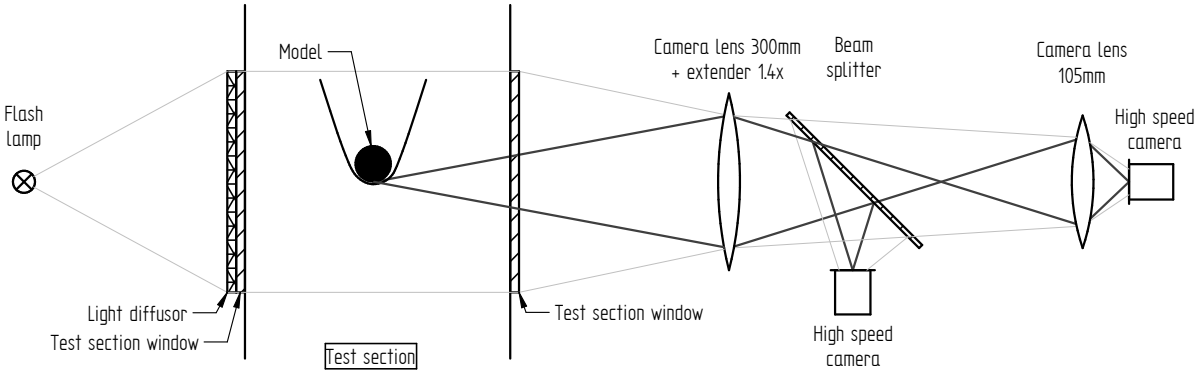

Fig 2. Optical setup

Two videos are obtained for each test. They are analysed with an image post-treatment algorithm, as shown in Figure 3. First, each frame is corrected for the model vibration by using a cross-correlation method. The low magnified video is used for this purpose. Each frame is cross-correlated to a reference image. Once the model displacement caused by the vibration is known, the vibration correction is then propagated to the highly magnified video using the ratio of the two magnifications. Then, the videos are normalized with a median filter and a gray-scale dilation. Finally, the model contour is extracted through a contour detection algorithm [8]. The ablation profile is computed by measuring the distance between the model contour of each frame from that of the initial state at the steady flow start.

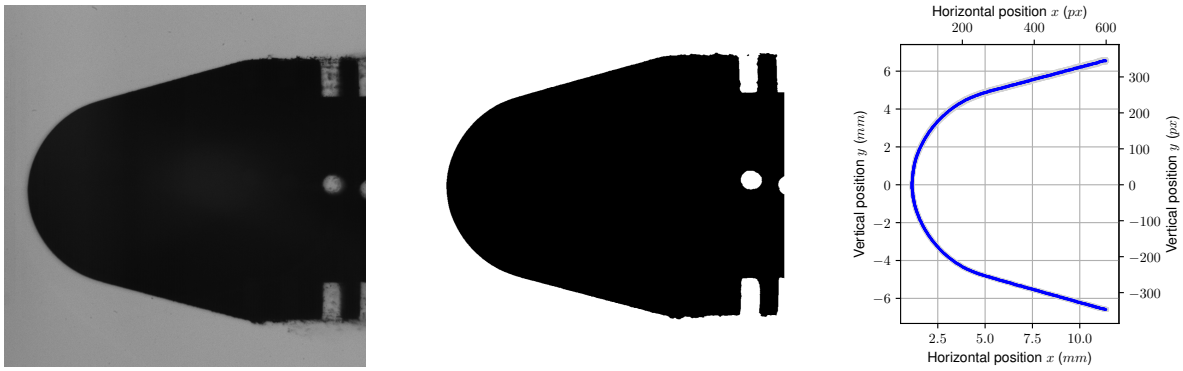

(a) Raw image **(b)** Normalized image **(c)** Extracted contour

Fig 3. Images from the post-processing

3. Results

The post-test observations confirm that the gallium model is ablated by melting. The model surface is modified by the flow and re-solidified gallium bubbles are also visible on the sides of the model. A comparison of a gallium model before and after the test is presented in Figure 4.

(a) Before testing **(b)** After testing

Fig 4. 10mm-hemisphere-cone models before and after testing at Mach 4.5, $h = 3km$

The duration between the test start and the onset of ablation, also defined as the heating phase duration, is measured from the recorded videos and presented in Table 3. The heating phase duration is reduced when the flow enthalpy increases. The heating phase duration for condition $h = 13km$ with the lowest enthalpy exceeds the steady flow duration, so the ablation process could not be evaluated.

Table 3. Heating phase durations

h (km)	Model geometry ($-$)	Heating phase duration (ms)
1	Hemisphere ∅10mm-cone	0.4
3	Hemisphere ∅8mm-cone	0.5
3	Hemisphere ∅10mm-cone	0.5
3	Hemisphere ∅14mm-cylindre	0.4
6	Hemisphere ∅10mm-cone	0.9
13	Hemisphere ∅10mm-cone	n/a

The ablation profiles obtained at the end of the steady flow for the flow condition $h = 3km$ is shown in Figure 5. Similar profiles are measured for the flow condition $h = 1km$. However, for the flow condition $h = 6km$, the surface recession caused by the ablation is evaluated at about one pixel and so is too small to be precisely measured by the direct visualization setup.

The pattern of the ablation profiles is similar for all models. The maximum of the surface recession is not located at the stagnation point but rather at a location $30°$ from the hemisphere symmetry axis. The surface recession at the stagnation point is only a local maximum such that the surface recession slightly decreases or remains constant up to a position of $10 - 20°$. Downstream this position, the surface recession increases rapidly until it achieves a maximum near $30°$. After this position, the surface recession monotonically decreases. Downstream of $60°$, the thickness of the gallium liquid layer becomes noticeable on the videos. This leads to an erroneous surface recession measurement beyond this position.

Regarding the symmetry of the gallium model, the symmetric shape is globally conserved during the ablation process. The ablation starts on a side of the model but propagates quickly over the entire stagnation surface.

4. Discussions

The observed ablation pattern correspond to the characteristic ablation profile in a high density flow. In addition, similar profiles for the ablation by melting have been reported for different materials and different facilities ([1] & [3]). In the ISL hyperballistic tunnel, ablated aluminium spheres after a hypersonic decelerated free flight show a conical forebody as shown in Figure 6a. In a wind tunnel, Silton & Goldstein observed that the ablation starts on the side of the stagnation point of a water ice model as shown in Figure 6b. The main conditions of these experiments are summarized in Table 4. Despite the different facilities and the different ablative materials, the Reynolds number is about $5E + 5$ to $4E + 6$. The locations of the maximum ablation are measured respectively at $30°$ for Luneau's experiments [1] and at $45°$ for Silton & Goldstein's experiments [3]. In these study, the contribution of the laminar-turbulent transition in the boundary layer is emphasised to explain the position of the maximum ablation.

Table 4. Freestream conditions for the ablation experiments

Experiment (-)	Material (-)	Facility (-)	M_∞ (-)	Re_∞ (-)	$\theta_{ablation,max}$ (°)
Present work	Gallium	Shock tunnel	4.5	$[5E+5; 1E+6]$	$30° \pm 10°$
Luneau [1]	Aluminium	Hyperballistic tunnel	$[9; 16]$	$[3E+6; 4E+6]$	$30° \pm 5°$
Silton & Goldstein [3]	Water ice	Wind tunnel	5	$1E+6$	$45° \pm 5°$

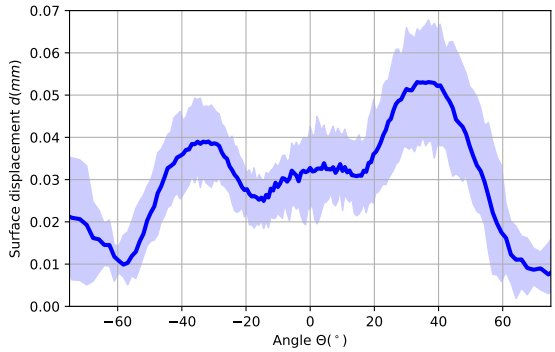

(a) 8mm-hemisphere

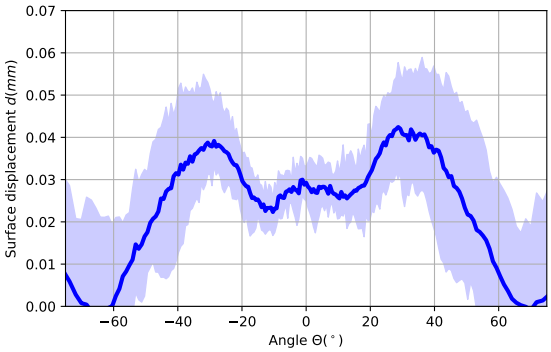

(b) 10mm-hemisphere

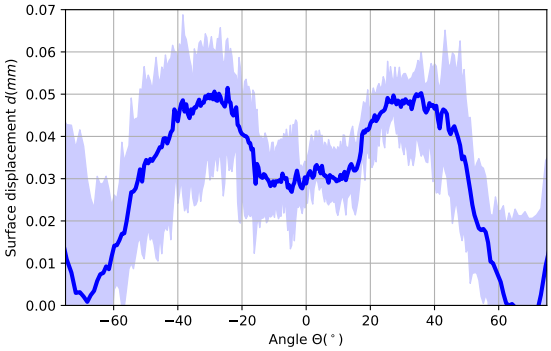

(c) 14mm-hemiphere

Fig 5. Ablation profiles at $t = 2ms$ for the flow condition Mach 4.5 and $h = 3km$ with the uncertainties represented by the blue areas

(a) Ablated aluminium sphere after a free flight test [1]

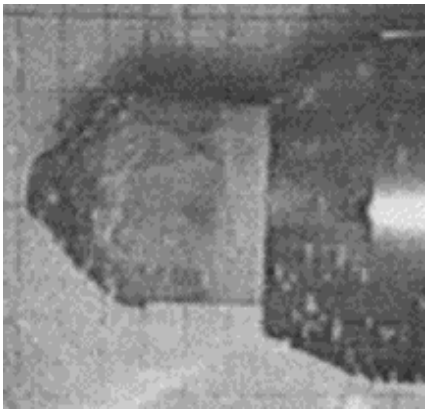

(b) Ablated water ice model in a supersonic wind tunnel [3]

Fig 6. Comparison of ablation profiles obtained with various facilities and model materials

4.1. Liquid ablation profile

The gallium ablation experiments are reproduced with CFD simulations. The solver used is the ablationFOAM solver, which is an OpenFOAM solver developed at ISL and dedicated to the simulation of the wall heat flux and the ablation by melting in hypersonic flows. Solver validations are performed with wall heat flux measurements previously performed in the ISL shock tunnels.

For the ablation simulations, the computational mesh is an axisymmetric mesh. The flow is modelled as a nitrogen flow with vibrational excitation but without chemical reaction. In order to determine the contribution of the flow turbulence to the ablation by melting, three simulations with three turbulence conditions are used:

- The first simulation is performed with laminar flow conditions. No turbulence model is used.
- The second simulation is performed with a two-equation turbulence model, the $k-\omega\ SST$ model [9], which models the turbulence but does not model the laminar-turbulent transition.
- The third simulation is performed with a four-equation turbulence model, the $k-\omega\ SST\ \gamma-Re_\theta$ model [10]. It models the turbulence and the laminar-turbulent transition based on user-defined correlations. However, the default correlation generates a transition too sensitive to the freestream turbulence parameters. Therefore, this turbulence model with this default correlation is unusable for a reliable simulation of the gallium ablation simulations. For that reason, the results obtained with this turbulence model are not presented in the following.

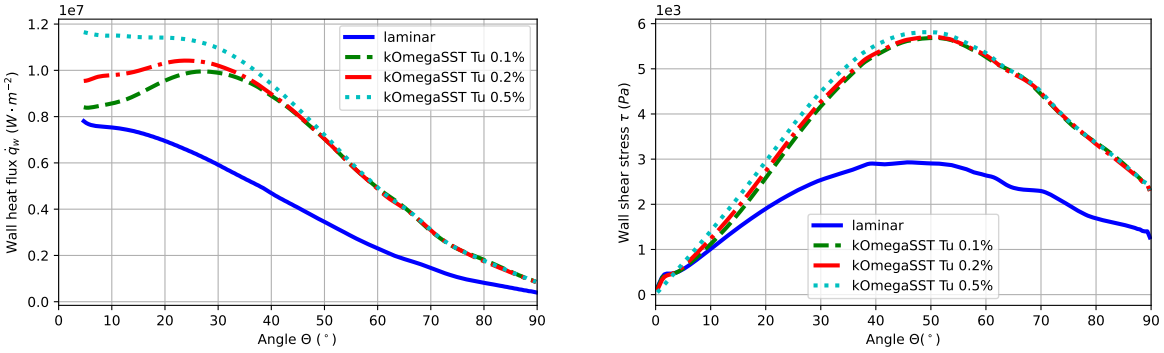

(a) Wall heat flux profiles

(b) Wall shear stress profiles

Fig 7. Profiles for the 14mm-hemisphere-cylinder for the flow condition Mach 4.5 and $h = 3km$

Figure 7a shows the simulated wall heat flux profiles on the $14mm$ gallium hemisphere for the flow condition Mach 4.5 and $h = 3km$. As expected the wall heat flux for the laminar case is lower than the one for the turbulent cases. Previous studies performed with a $100mm$ hemisphere in the ISL shock tunnel show that the boundary layer can become turbulent near the positions $10°$-$20°$. The wall heat flux profiles for the cases with low freestream turbulence intensities present a profile similar to the ablation profiles. First, the wall heat flux increases downstream of the stagnation point, then reaches a maximum at the position $30°$. Even if this turbulence model does not model the laminar-turbulence transition, it shows that the contribution of the turbulent wall heat flux becomes significant downstream the position of $10°$. As consequence the total wall heat flux, i.e. the sum of the laminar and the turbulent wall heat flux, increases and presents a maximum at $30°$.

Similarly the wall shear stress profiles are compared for the laminar and the turbulent cases. For both cases, the profiles present a similar shape with a maximum located near the position $50°$. The wall shear stress is higher for the turbulent cases than for the laminar one. However, the maximal shear stresses never exceeds a value of $6kPa$ and therefore are much lower than the tensile stress of the gallium

material, which is around 8-$25MPa$ as presented in Table 2. Thus, the ablation by erosion caused by the wall shear stress cannot be the main phenomenon for the ablation by melting in a dense flow and is only a secondary phenomenon.

The evolutions of the velocity, the temperature and the turbulence parameters along the model surface for the $k-\omega\ SST$ turbulence model are shown in Figure 8. Boundary layer profiles obtained numerically are presented for several angular positions θ on the hemisphere. As expected the velocity along the model surface increases and the temperature decreases as the distance from the stagnation point decreases. An increase of the turbulence kinetic energy is simulated downstream the stagnation point as shown in Figure 8c. The development of the turbulence starts after a position of $10°$, where the laminar-turbulent transition is expected based on the experimental ablation profiles. These CFD results indicate the possibility of the boundary layer to become turbulent in this region. The transition to the turbulence induces a turbulent wall heat flux, which enhances the wall heat flux and finally the ablation.

4.2. Ablation start time

The Table 3 compares the ablation start time obtained by the CFD simulations with the gallium ablation experiments. The numerical results provide a time interval because of the ablation model used, which is dependant of the first cell size on the ablated surface. Despite this, the numerical and experimental ablation start times are of the same order of magnitude. This finally confirms the ability of the numerical solver to predict the ablation start time measured experimentally in an impulse facility.

Table 5. Ablation start time

Condition n°	h (km)	D (mm)	Numerical start time (ms)	Experimental start time (ms)
1	3	14	0.1-0.7	0.4
1	3	10	0.1-0.3	0.5
2	1	14	0.1-0.7	0.4
3	6	14	0.3-1.5	0.9
4	13	14	>2	n/a

5. Conclusion

A new experimental method for the measurement of the liquid ablation in a hypersonic shock tunnel has been developed. The combination of gallium as a low temperature ablator with the direct visualization measurement method allows precise measurements of liquid ablation profiles in dense flows despite the experiment duration of only two milliseconds. The characteristic liquid ablation profile in a dense flow is measured. The position of the maximum ablation is never located at the stagnation point but is shifted toward the location $30°$. This observation is in agreement with previous studies reported in the literature.

Finally, numerical results are compared to the experimental ablation profiles. They highlight that the ablation by erosion caused by the wall shear stress is a secondary phenomenon in the present ablation experiments. In contrary, the wall heat flux profile shows a similar maximum shift for the turbulent simulations with a low freestream turbulent intensity. A rapid turbulence development downstream the position $10°$ is simulated. This enhances the assumption of a laminar-turbulent transition in the boundary layer, which controls the shapes of the wall heat flux profiles and thus of the ablation profiles.

The gallium ablation experiment provides data for the validation of numerical tools dedicated to the ablation prediction. It provides the ablation start time and the ablation profile. The ablation measurements will be further investigated within the ISL hyperballistic tunnel, which allows the study of the liquid ablation with metallic materials such as tungsten or Inconel up to a free flight velocity of $9km \cdot s^{-1}$.

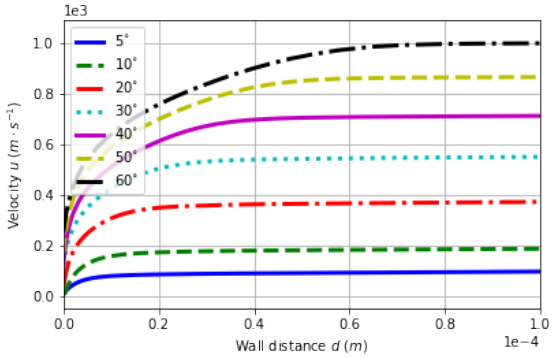

(a) Velocity profiles

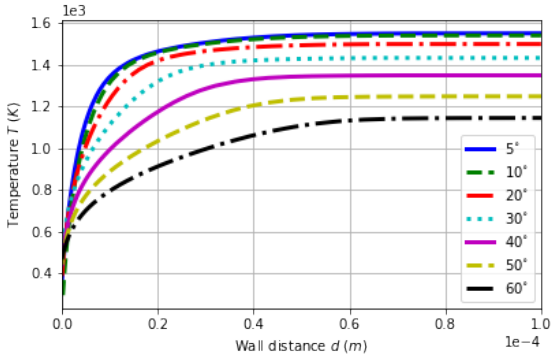

(b) Temperature profiles

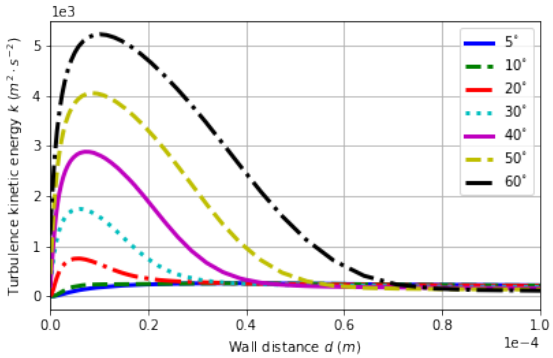

(c) Turbulence kinetic energy profiles

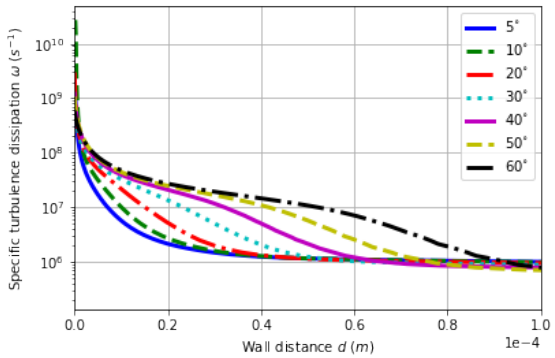

(d) Specific turbulence dissipation profiles

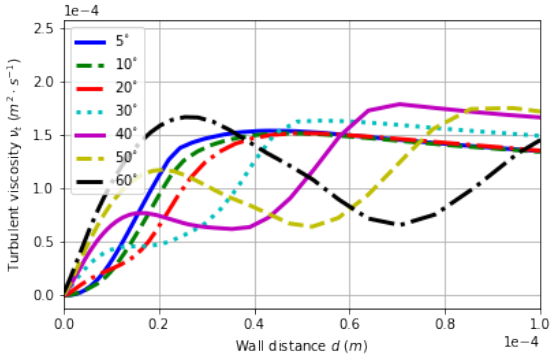

(e) Turbulent viscosity profiles

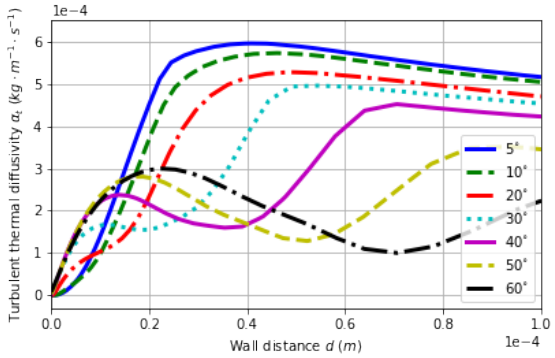

(f) Turbulent thermal dissipation profiles

Fig 8. Boundary layer profiles for the 14mm-hemisphere-cylinder at Mach 4.5, $h = 3km$ and freestream turbulence intensity of 0.2%

References

[1] J. Luneau, *Contribution à l'étude des phénomènes aérothermiques liés au vol hypersonique décéléré*. PhD thesis, Institut franco-allemand de recherches de Saint-Louis, 1969. (in French).

[2] J. M. Bridges and R. N. Pinchok, "An experimental investigation of the re-entry behavior of metals and alloys," *Westinghouse Astronuclear Laboratory*, 1964, https://doi.org/10.2172/4240354.

[3] S. I. Silton and D. B. Goldstein, "Ablation onset in unsteady hypersonic flow about nose tip with cavity," *Journal of thermophysics and heat transfer*, vol. 14, no. 3, pp. 421–434, 2000, https://doi.org/10.2514/2.6540.

[4] D. Callaway, M. Reeder, R. Greendyke, and R. Gosse, "Photogrammetric measurement of recession rates of low temperature ablators in supersonic flow," *48th AIAA Aerospace Sciences Meeting*, 2010, https://doi.org/10.2514/6.2010-1216.

[5] C. S. Combs, N. T. Clemens, P. M. Danehy, and S. M. Murman, "Heat-shield ablation visualized using naphthalene planar laser-induced fluorescence," *Journal of Spacecraft and Rockets*, vol. 54, no. 2, pp. 476–494, 2017, https://doi.org/10.2514/1.A33669.

[6] "Thermochemical tables, Gallium (Ga)," *NIST-JANAF*, 1998.

[7] S. Ayrinhac, "Compilation of thermodynamic and elastic data of liquid Ga," *UPMC, Sorbonne Universités*, 2000.

[8] S. Suzuki and K. Abe, "Topological structural analysis of digitized binary images by border following," *Computer Vision, Graphics, and Image Processing*, vol. 30, no. 1, pp. 32–46, 1985, https://doi.org/10.1016/0734-189X(85)90016-7. https://doi.org/10.1016/0734-189X(85)90016-7.

[9] OpenCFD, "OpenFOAM API guide v2012: kOmegaSST," 2022. https://www.openfoam.com/documentation/guides/latest/api/classFoam_1_1RASModels_1_1kOmegaSST.html.

[10] OpenCFD, "OpenFOAM API guide v2012: kOmegaSSTLM," 2022. https://www.openfoam.com/documentation/guides/latest/api/classFoam_1_1RASModels_1_1kOmegaSSTLM.html.